sustainability

MDPI

Article

β-Cyclodextrin/Graphene Oxide Multilayer Composite Membrane: A Novel Sustainable Strategy for High-Efficiency Removal of Pharmaceuticals and Personal Care Products

Ziyang Zhang [1,*], Ying Yang [2], Zibo Tang [3], Fangyuan Liu [4] and Hongrui Chen [5]

[1] Beijing Energy Conservation & Sustainable Urban and Rural Development Provincial and Ministry Co-Construction Collaboration Innovation Center, Beijing 100044, China
[2] Key Laboratory of Urban Stormwater System and Water Environment, Ministry of Education, Beijing University of Civil Engineering and Architecture, Beijing 102616, China; waiwai051700@163.com
[3] Beijing Engineering Research Center of Sustainable Urban Sewage System Construction and Risk Control, Beijing University of Civil Engineering and Architecture, Beijing 100044, China; tang_zibo@126.com
[4] Beijing SDL Technology Co., Ltd., Beijing 102206, China; liufangyuan@chsdl.com
[5] CRRC Environmental Science & Technology Cooperation, Beijing 100067, China; hr630@126.com
* Correspondence: ziyangzhang@126.com

Abstract: The efficient removal of pharmaceuticals and personal care products (PPCPs) from aqueous solutions using conventional adsorbents is hindered by low adsorption capacity, insufficient selectivity, poor regeneration performance, and limited stability. In this study, a multilayer β-CD/GO membrane was successfully prepared via layer-by-layer coating with β-cyclodextrin (β-CD) and graphene oxide (GO). The multilayer β-CD/GO membrane combines the host–guest complexation ability of β-CD with the abundant oxygen-containing functional groups of GO to enhance the targeted removal of PPCPs (CTD, SMZ, and DCF) from aqueous solutions. The prepared multilayer β-CD/GO membrane adsorbent overcomes the separation difficulties and poor regeneration performance of powdered adsorbents, and the multilayer structure can significantly enhance structural stability and increase the number of adsorption sites. Batch adsorption experiments showed that the optimal adsorption performance of the multilayer β-CD/GO membrane for PPCPs occurred at pH 4 and in the absence of coexisting ions. With increasing pH values in the range of 4–9, the adsorption capacities of CTD, SMZ, and DCF slightly decreased to 14.37, 13.69, and 13.01 mg/g, respectively, and the adsorption capacities decreased slowly to 4.88, 3.51, and 3.26 mg/g as the coexisting ion concentrations increased from 0 to 0.20 mol/L. The adsorption mechanism of the multilayer β-CD/GO membrane for PPCPs was systematically investigated through adsorption kinetics, isotherms, and thermodynamics. The adsorption processes of CTD, SMZ, and DCF by the multilayer β-CD/GO membrane were well described by both pseudo-first-order and pseudo-second-order kinetic models ($R^2 > 0.984$), suggesting a hybrid adsorption mechanism involving both physisorption and chemisorption. The isotherm results indicated that the adsorption of CTD by the multilayer β-CD/GO membrane followed the Langmuir model ($R^2 = 0.923$), whereas the adsorption of SMZ and DCF was better described by the Freundlich model ($R^2 = 0.984$–0.988). The multilayer β-CD/GO membrane exhibited high adsorption capacities for CTD, SMZ, and DCF with maximum capacities of 35.56, 43.29, and 39.49 mg/g, respectively. Thermodynamic analyses indicated that the adsorption of PPCPs was exothermic ($\Delta H^0 = -86.16$ to -218.49 J/mol/K) and non-spontaneous ($\Delta G^0 = 9.84$–11.56, 9.50–12.54, and 10.09–14.46 kJ/mol). The multilayer β-CD/GO membrane maintained a removal efficiency of over 58.45–71.73% for CTD, SMZ, and DCF after five consecutive regeneration cycles, demonstrating high reusability for practical applications. The adsorption mechanisms of the multilayer β-CD/GO membrane include electrostatic interactions, hydrogen bonding, hydrophobic interactions, and π-π

check for updates

Academic Editor: Francisco José Hernández Fernández

Received: 19 March 2025
Revised: 1 April 2025
Accepted: 3 April 2025
Published: 8 April 2025

Citation: Zhang, Z.; Yang, Y.; Tang, Z.; Liu, F.; Chen, H. β-Cyclodextrin/Graphene Oxide Multilayer Composite Membrane: A Novel Sustainable Strategy for High-Efficiency Removal of Pharmaceuticals and Personal Care Products. *Sustainability* **2025**, *17*, 3322. https://doi.org/10.3390/su17083322

Copyright: © 2025 by the authors. Licensee MDPI, Basel, Switzerland. This article is an open access article distributed under the terms and conditions of the Creative Commons Attribution (CC BY) license (https://creativecommons.org/licenses/by/4.0/).

EDA interactions. This study offers a promising and environmentally friendly adsorbent for the efficient removal of PPCPs from aqueous solutions.

Keywords: PPCPs; adsorption; β-cyclodextrin; graphene oxide; removal efficiency

1. Introduction

The residual presence of pharmaceuticals and personal care products (PPCPs) in water bodies has raised global concerns [1]. PPCPs continuously enter aquatic environments through pathways such as wastewater treatment plant discharge and stormwater runoff [2,3]. Although PPCPs are detected in aquatic environments at concentrations ranging from ng/L to μg/L [4,5], they can potentially be significantly harmful to ecosystem structure, which may be attributed to bioaccumulation, potential biological activity, and persistence [3,5]. For example, PPCPs can disrupt the endocrine systems of aquatic organisms [4], induce resistance in microorganisms [6], and potentially threaten human health through the food chain [7]. Characterized by chemical stability and low biodegradability, PPCPs are not efficiently removed by conventional wastewater treatment processes [8]. Therefore, exploring efficient and reliable techniques to remove PPCPs from aquatic environments is essential.

Various techniques have been reported for the removal of PPCPs from aqueous environments, including advanced oxidation processes [9], photocatalytic degradation [10], biological treatment [11], adsorption [12], non-thermal plasma treatment [13], and coagulation [14]. With the advantages of operational simplicity, high efficiency, and low cost, adsorption demonstrates better potential for application among these treatment techniques [15]. To date, adsorbents such as activated carbon [16], zeolites [17], alumina [18], and bentonite [19] have been widely utilized for the adsorption of contaminants in aqueous environments. However, the practical applications of these adsorbents are constrained by their poor stability, low adsorption capacity, and insufficient selectivity. Moreover, traditional adsorbents are mostly in powder form, which makes them difficult to recover and costly to regenerate. Therefore, it is crucial to develop adsorbents with high stability, large adsorption capacity, targeted selectivity, and excellent regeneration performance.

β-cyclodextrin (β-CD) is a cyclic oligosaccharide obtained by the enzymatic conversion of starch, consisting of seven D-glucopyranose units connected via α-1,4-glycosidic bonds to form a hollow cylindrical three-dimensional ring structure [20,21]. β-CD possesses a unique supramolecular structure characterized by a hydrophilic outer surface and a hydrophobic inner cavity [22]. The hydrophobic inner cavity as a host enables selective host–guest complexation with organic contaminant guests through complementary polarity interactions [23]. Furthermore, β-CD exhibits numerous advantages, including wide availability, non-toxicity, low cost, and biodegradability [21]. However, the low mechanical strength of β-CD in aqueous solutions hinders its recovery. Graphene oxide (GO) possesses a two-dimensional layered structure [24], and its abundant oxygen-containing functional groups can adsorb contaminants through electrostatic interactions, hydrogen bonding, hydrophobic interactions, and π-π interactions [25–27]. However, GO is prone to aggregation, which reduces the specific surface area and adsorption sites, leading to a decrease in adsorption capacity. To enhance stability and adsorption performance, β-CD and GO were composited and prepared into multilayer membrane adsorbents using a coating method. The prepared multilayer β-CD/GO membrane adsorbent overcomes the separation difficulty and poor regeneration performance of powdered adsorbents. The multilayer structure of the β-CD/GO membrane, formed through interlayer stacking, can significantly improve the structural stability of the adsorbent and increase the number

of adsorption sites. Given the advantages of the multilayer β-CD/GO membrane, the effectiveness and underlying mechanisms of its adsorption for PPCPs were investigated.

In this study, a multilayer β-CD/GO membrane was first successfully prepared via layer-by-layer coating with a homogeneously dispersed solution of β-cyclodextrin and graphene oxide, and then it was employed to adsorb PPCPs in aqueous solutions. Three representative PPCPs were selected, including Cimetidine (CTD), Sulfamethoxazole (SMZ), and Diclofenac (DCF). SEM and AFM were used to characterize the multilayer β-CD/GO membrane. The effects of pH values, contact time, initial concentration, temperature, and coexisting ions on the adsorption capacity of PPCPs were systematically investigated. The experimental data were analyzed using kinetic and isotherm models to investigate the adsorption mechanisms. In addition, the regeneration performance of the multilayer β-CD/GO membrane was investigated to demonstrate its economic and environmental properties. This study presents a novel approach for the efficient and stable removal of PPCPs from aqueous solutions, contributing to the development of the adsorbent materials field by designing a multilayer membrane adsorbent.

2. Materials and Methods

2.1. Materials

Cimetidine (CTD), sulfamethoxazole (SMZ), and Diclofenac (DCF) were bought from Sigma Aldrich, whose molecular structures are shown in Figure 1. Methanol, acetonitrile, and acetone were purchased from Merck. Sulfuric acid, anhydrous ethanol, sodium hydroxide, potassium permanganate, potassium bromide, β-cyclodextrin, graphite powder (8000 mesh), and polymethyl methacrylate (PMMA) were purchased from Sinopharm Chemical Reagent Co., Ltd. (Shanghai, China). Copper foil was purchased from Saiwei Metal Materials Co., Ltd. (Xingtai, China) with a purity of 99.99%. All the above reagents and solvents were of analytical grade. The aqueous solutions were prepared with ultra-pure water.

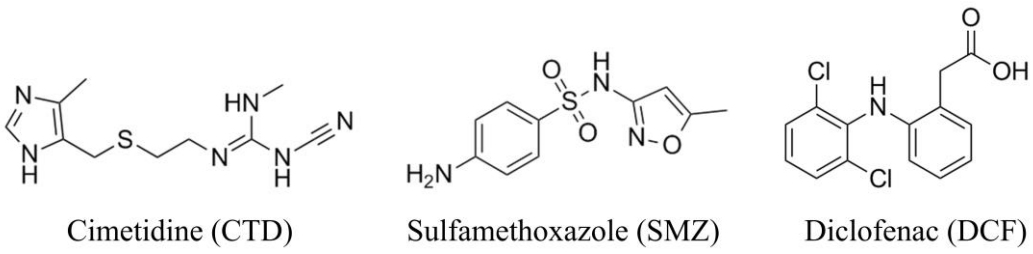

Figure 1. Molecular structures of CTD, SMZ, and DCF.

2.2. Synthesis of Adsorbents

2.2.1. Preparation of GO

Graphene oxide was prepared using the modified Hummers method [28]. Firstly, 2.5 g of graphite powder, 1.0 g of $NaNO_3$, and 60.0 mL of H_2SO_4 were placed in a three-neck flask, followed by thorough stirring in an ice bath for 30.0 min. Then, 10.0 g of $KMnO_4$ was added slowly to the mixture and stirred for 60 min. The mixture was then moved to an oil bath at 40 °C for 30 min. Subsequently, 115.0 mL ultra-pure water was slowly added, and the mixture was stirred at 98 °C for 5 min; 30% H_2O_2 was then added to the mixture until no bubbles were formed. The mixture was then centrifuged at 3500 rpm for 10 min. The resulting precipitate was washed with ultra-pure water and 5% HCl until the pH was neutral. Finally, graphene oxide was obtained by drying at 60 °C for 48 h.

2.2.2. Preparation of Multilayer β-CD/GO Membrane

The preparation process for the multilayer β-CD/GO membrane is shown in Figure 2. Four grams of NaOH and ten grams of β-CD were completely dissolved in 200.0 mL of

ultra-pure water and maintained at 80 °C for 0.5 h. At the same time, 500.0 mg of prepared GO was added to 200.0 mL of ultra-pure water for ultrasonic dissolution. The above two solutions were mixed and maintained at 80 °C for 3.0 h. Finally, the mixture was reacted at 50 °C for 1.5 h and washed five times by centrifugation at 3500 rpm for 10.0 min. Finally, a homogeneous dispersion of the β-CD/GO mixture was obtained.

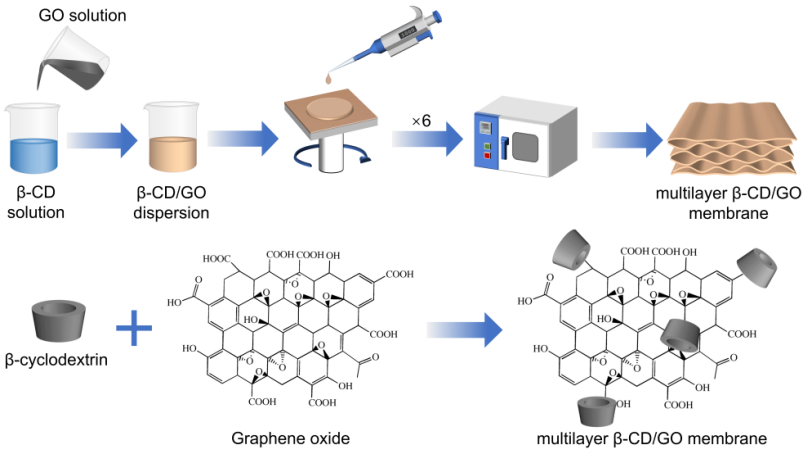

Figure 2. Schematic preparation process of multilayer β-CD/GO membrane.

Copper foil 0.1 mm thick was cut into 30 mm × 30 mm square sheets. Then, the sheets were sonicated in acetone, anhydrous ethanol, and ultra-pure water for 10.0 min, respectively. Finally, the copper sheets were washed with ultra-pure water and dried overnight.

A total of 1.0 mL of the β-CD/GO homogeneous dispersion was uniformly coated and dried on the copper foil. The coating and drying processes were repeated six times. In addition, a layer of PMMA–methanol solution was applied between the third and fourth coatings to improve the mechanical strength of the membrane. Then, the samples were dried at 60 °C for 2.0 h. Finally, a multilayer β-CD/GO membrane was prepared by stripping the samples from the copper foil.

2.3. Characterization

The surface and cross-section morphologies of the multilayer β-CD/GO membrane were investigated using scanning electron microscopy (SEM, SU4800, Hitachi, Tokyo, Japan) with a 5 kV accelerated electron beam. Atomic force microscopy (AFM, Veeco Digital Instruments Dimension 3100, Irvine, CA, USA) was employed to measure the surface roughness of the multilayer β-CD/GO membrane.

2.4. Adsorption Experiments

Batch adsorption experiments were used to study the effects of different factors on the removal of CTD, SMZ, and DCF by the multilayer β-CD/GO membrane, including solution pH value, contact time, initial concentration, and temperature. Briefly, 30 mg of multilayer β-CD/GO membrane was added to a beaker containing 30 mL of a PPCP solution with an initial concentration of 20 mg/L. The beaker was transferred to a thermostatic oscillator and shaken at 298 K and 160 rpm for 24 h. The effect of pH was investigated by adjusting the solution pH values from 4 to 9 using 0.1 M NaOH and 0.1 M HCl. To study the effect of contact time, the residual concentrations of PPCPs were detected at predetermined time points (0, 3, 6, 9, 12, 16, 20, 25, 30, 40, 50, 60, 80, 120, 180, 270, 360, 540, 720, and 1440 min) during the adsorption process. The initial PPCP solution concentrations varied in the range of 1.0 to 40.0 mg/L to investigate the adsorption isotherms of the multilayer β-CD/GO membrane. To examine the influence of temperature on adsorption capacity,

experiments were conducted at different temperatures of 298 K, 308 K, and 318 K. In addition, the impact of different coexisting ions on the adsorption performance of the multilayer β-CD/GO membrane was studied, including NaCl, Na_2CO_3, and $CaCl_2$. The concentration of coexisting ions ranged from 0 to 0.20 mol/L. The concentration of PPCPs in an aqueous solution was determined by ultra-performance liquid chromatography (ACQUITY UPLC-H Class, Waters, MA, USA).

After the adsorption experiment, the adsorbed multilayer β-CD/GO membrane was washed by stirring with ultra-pure water at 105 rpm for 24 h and then dried for 12 h to obtain the regenerated multilayer β-CD/GO membrane. The reusability of the multilayer β-CD/GO membrane was evaluated through five consecutive cycles of adsorption–desorption processes.

The adsorption capacity of the multilayer β-CD/GO membrane for PPCPs was calculated by Equation (1):

$$q_t = \frac{(C_0 - C_t)V}{m}, \quad (1)$$

where q_t (mg/g) is the adsorption capacity of multilayer β-CD/GO membrane for PPCPs at time t, C_0 (mg/L) is the initial concentration of the PPCP solution, C_t (mg/L) is the concentrations of the PPCP solution at time t, V (L) is the volume of the PPCP solution, and m (g) is the mass of the multilayer β-CD/GO membrane.

3. Results and Discussion

3.1. Characterization of Multilayer β-CD/GO Membrane

The surface and cross-section images of the multilayer β-CD/GO membrane were investigated using SEM, and the results are shown in Figure 3. As shown in Figure 3a, the multilayer β-CD/GO membrane possessed a continuous and integrated surface. Furthermore, the surface of the multilayer β-CD/GO membrane exhibited a significantly rough and wrinkled morphology. Figure 3b demonstrates that the multilayer β-CD/GO membrane exhibits a tight and multilayered stacking structure with uniformly distributed layers, which could enhance its stability in aqueous solutions. The surface roughness of the multilayer β-CD/GO membrane is depicted in Figure 3c. The image displayed significant fluctuations on the surface of the β-CD/GO membrane [29], which is consistent with the results observed via SEM. The rougher surface indicated that the multilayer β-CD/GO membrane was equipped with a large specific surface area, which could expose abundant available adsorption sites for the adsorption of PPCPs.

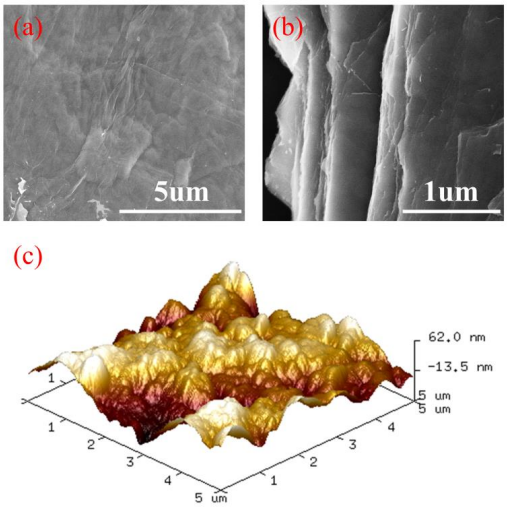

Figure 3. (**a**) SEM surface image; (**b**) SEM cross-section image; and (**c**) AFM image of multilayer β-CD/GO membrane.

3.2. Effect of pH Values

The effect of solution pH values on the adsorption capacity of multilayer β-CD/GO membrane for PPCPs was presented in Figure 4. The results demonstrated that the adsorption capacity of PPCPs onto multilayer β-CD/GO membrane was enhanced under acidic conditions. With increasing pH values, the adsorption capacity decreased slightly. The maximum adsorption capacities of the multilayer β-CD/GO membrane for CTD, SMZ, and DCF at pH 4 were 18.36, 16.66, and 15.35 mg/g, respectively. When the pH value was increased to 9, the adsorption capacities for CTD, SMZ, and DCF decreased to 14.37, 13.69, and 13.01 mg/g, respectively.

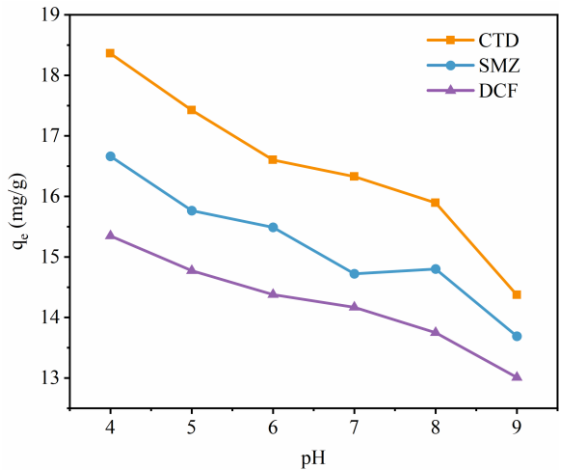

Figure 4. Effects of pH values on the adsorption of CTD, SMZ, and DCF onto the multilayer β-CD/GO membrane.

The influence of solution pH values on the adsorption capacity of the multilayer β-CD/GO membrane may be attributed to changes in the surface charge of the membrane and the form of PPCPs in solution [30]. According to a previous study, the zeta potential value of β-CD/GO composite was negative within the pH range of 4–9 [31]. The possible adsorption mechanisms of multilayer β-CD/GO membrane for CTD, SMZ, and DCF are schematically illustrated in Figure 5. For CTD, which has a pKa of 6.8, two dissociated species exist at different pH values, namely CTD^+ (pH < 6.8) and CTD^- (pH > 6.8) [32]. At pH < 6.8, CTD was easily adsorbed onto the membrane surface due to the electrostatic attraction between the negatively charged multilayer β-CD/GO membrane surface and CTD^+ molecules. Furthermore, the -NH- group in CTD formed hydrogen bonds with the abundant oxygen-containing functional groups on the multilayer β-CD/GO membrane surface [33], which played an important role in the adsorption of CTD. The $-CH_3$ group in CTD was considered a hydrophobic group, thereby enhancing the adsorption of CTD via hydrophobic interactions with the β-CD/GO membrane [34]. With increasing pH values from 4 to 9, the electrostatic attraction between CTD and the negatively charged multilayer β-CD/GO membrane surface transformed into electrostatic repulsion due to the conversion of CTD^+ to CTD^- in the solution, resulting in a reduced adsorption capacity for CTD.

SMZ is an amphoteric molecule, and its existence form can be easily altered with solution pH values, including SMZ^+ (pH < 1.6), SMZ^0 (1.6 < pH < 5.7), and SMZ^- (pH > 5.7) [35,36]. Previous studies have repeatedly mentioned that interactions between aromatic pollutants and carbonaceous adsorbents can occur via the π-π electron donor–acceptor (EDA) mechanism at lower pH values [37,38]. SMZ was considered a π-electron acceptor due to the strong electron-withdrawing ability of the sulfonamide group and the high electronegativity of the O atom within SMZ, which resulted in the two aromatic rings being electron-deficient [39]. In addition, the protonated amino

group (-NH_3^+) was confirmed to enhance the electron-accepting ability of SMZ [40]. The multilayer β-CD/GO membrane was used as a π-electron donor due to the π-electron-rich nature of graphene [41]. The adsorption of SMZ by the multilayer β-CD/GO membrane can be attributed to the π-π EDA interaction between the multilayer β-CD/GO membrane and SMZ at pH 4–5.7. In addition to π-π EDA interaction, hydrophobic interactions and hydrogen bonds between the -CH_3, -NH_2, and -NH- groups in SMZ and the multilayer β-CD/GO membrane also contributed to the adsorption of SMZ, which is consistent with previous research findings [33,34,36]. With increasing pH values from 5.7 to 9, the electrostatic repulsion with the multilayer β-CD/GO membrane surface was enhanced due to the increase in the proportion of SMZ^- in solution, resulting in a decrease in adsorption capacity. Furthermore, the deprotonation of SMZ at high pH values reduced its π-electron-accepting ability and hydrophobicity, thereby reducing π-π EDA and hydrophobic interactions with the multilayer β-CD/GO membrane [42]. However, at pH 9, a large amount of SMZ was still adsorbed onto the multilayer β-CD/GO membrane due to charge-assisted hydrogen bond (CAHB) interactions [43,44]. This interaction involved SMZ^- withdrawing a proton from the solution to produce neutral SMZ^0, which then formed hydrogen bonds with the oxygen-containing functional groups on the multilayer β-CD/GO membrane surface [33,45].

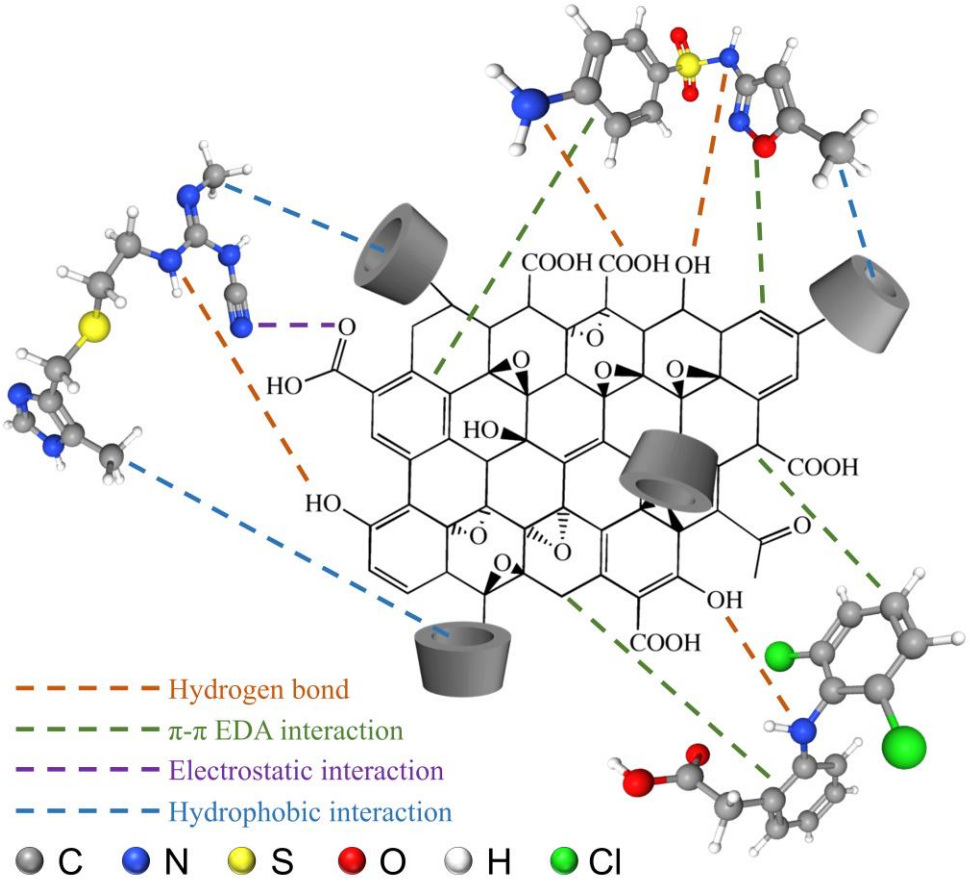

Figure 5. Schematic diagram of the adsorption mechanisms of the multilayer β-CD/GO membrane.

The pKa of DCF is 4.2 [46], indicating that DCF mainly exists as DCF^- in the pH range of 4.2–9 in this study. Similarly, at pH 4.0, the adsorption of DCF by the multilayer β-CD/GO membrane was due to π-π EDA and hydrogen bond interactions between the aromatic rings and the -NH- group in DCF and the multilayer β-CD/GO membrane [36,37]. With increasing pH values from 4.2 to 9, the electrostatic repulsion between DCF^- molecules and the multilayer β-CD/GO membrane was enhanced, whereas hydrogen bonds and

π-π EDA interactions were weakened, which negatively impacted the adsorption capacity of DCF on the multilayer β-CD/GO membrane.

3.3. Adsorption Kinetics

The adsorption kinetics of CTD, SMZ, and DCF on the multilayer β-CD/GO membrane were determined, and the results are presented in Figure 6. According to Figure 6, CTD, SMZ, and DCF were rapidly adsorbed onto the multilayer β-CD/GO membrane within the first 120 min, which could be attributed to the existence of abundant available adsorption sites on the multilayer β-CD/GO membrane's surface [47]. The adsorption rate then slowed down due to the gradual saturation of the active sites and finally reached equilibrium at approximately 720 min. The equilibrium adsorption capacities of the multilayer β-CD/GO membrane for CTD, SMZ, and DCF were 19.06, 17.19, and 14.70 mg/g, respectively.

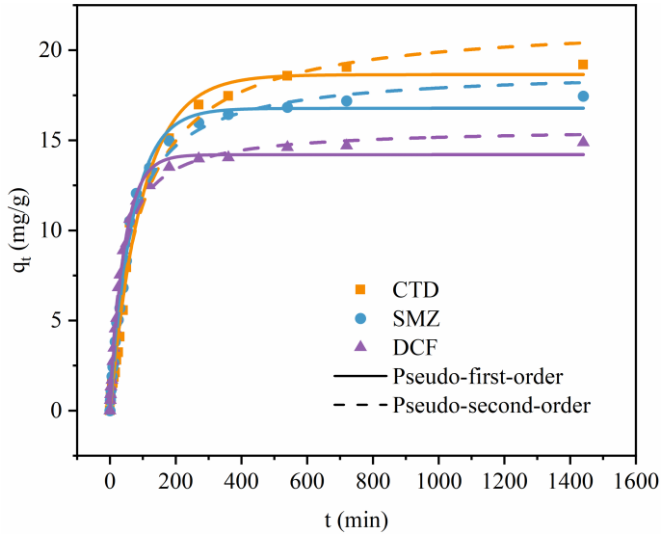

Figure 6. Adsorption kinetics of CTD, SMZ, and DCF onto the multilayer β-CD/GO membrane.

To investigate the adsorption mechanism, pseudo-first-order and pseudo-second-order models were applied to analyze the adsorption process of PPCPs on the β-CD/GO membrane. The corresponding equations for the above two models are presented in Equation (2) and Equation (3), respectively [48].

$$q_t = q_e\left(1 - e^{-k_1 t},\right) \tag{2}$$

$$q_t = \frac{k_2 q_e^2 t}{1 + k_2 q_e t}, \tag{3}$$

where q_e (mg/g) is the adsorption capacity at the equilibrium state, k_1 (1/min) is the pseudo-first-order model rate constant, and k_2 (g/mg·min) is the pseudo-second-order model rate constant.

The kinetic parameters are listed in Table 1. The regression correlation coefficient R^2 values of the pseudo-first-order and pseudo-second-order models fitting all the experimental data were 0.990–0.995 and 0.984–0.994, respectively. In addition, the equilibrium adsorption capacities of CTD, SMZ, and DCF, calculated by the pseudo-first-order and pseudo-second-order models, were 18.64–21.67, 16.77–18.94 and 14.21–15.68 mg/g, respectively, which were in better agreement with the experimental data. Therefore, both pseudo-first-order and pseudo-second-order models can effectively describe the adsorption

process, indicating a hybrid mechanism combining physisorption and chemisorption for the adsorption of CTD, SMZ, and DCF by the multilayer β-CD/GO membrane [48,49].

Table 1. Kinetic parameters of the multilayer β-CD/GO membrane for SMZ, CTD, and DCF adsorption.

Adsorption Kinetic Models	Parameters	PPCPs		
		CTD	SMZ	DCF
Experimental data	*qe,exp* (mg/g)	19.06	17.19	14.70
Pseudo-first-order	*qe,cal* (mg/g)	18.64	16.77	14.21
	k_1 (1/min)	0.618	0.883	1.395
	R^2	0.990	0.995	0.995
Pseudo-second-order	*qe,cal* (mg/g)	21.67	18.94	15.68
	k_2 (g/mg·min)	0.031	0.055	0.112
	R^2	0.984	0.992	0.994

3.4. Adsorption Isotherms

Figure 7 illustrates the adsorption isotherms of CTD, SMZ, and DCF on the multilayer β-CD/GO membrane. At a lower initial concentration of the PPCP solution, the steep slope observed in the isotherms indicated high adsorption efficiencies for CTD, SMZ, and DCF, which were due to the abundant adsorption sites on the multilayer β-CD/GO membrane's surface [50]. The adsorption capacities of the multilayer β-CD/GO membrane for CTD, SMZ, and DCF increased with the rising equilibrium concentration of PPCPs. This result was attributed to the higher collision frequency between PPCPs and available adsorption sites on the multilayer β-CD/GO membrane at higher concentrations [51]. Furthermore, the increase in the concentration of PPCPs in solution enhanced the driving force for PPCPs to overcome the mass transfer resistance between the aqueous and solid phases [52]. As the concentration of the PPCP solution further increased, the adsorption sites on the multilayer β-CD/GO membrane surface gradually became saturated, and the adsorption finally reached equilibrium.

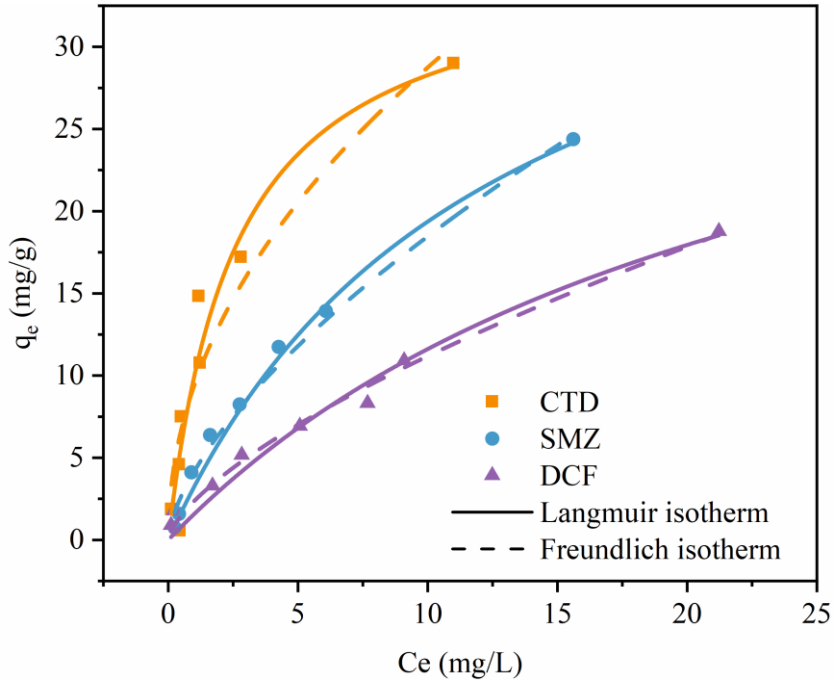

Figure 7. Adsorption isotherms of CTD, SMZ, and DCF onto the multilayer β-CD/GO membrane.

To reveal the interaction and determine the maximum adsorption capacity between the multilayer β-CD/GO membrane and PPCPs, the adsorption isotherm data of multilayer

β-CD/GO membrane were fitted using the Langmuir and Freundlich models, which are described in detail in Equations (4) and (5), respectively [53].

$$q_e = q_m \frac{K_L C_e}{1 + K_L C_e}, \quad (4)$$

$$q_e = K_F C_e^{1/n}, \quad (5)$$

where q_m (mg/g) is the maximum adsorption capacity, K_L is the Langmuir affinity constant, C_e (mg/L) is the concentration of PPCPs at the equilibrium state, K_F is the Freundlich constant, and $1/n$ is the adsorption intensity.

The isothermal fitting parameters are summarized in Table 2. For CTD, the correlation coefficient (R^2 = 0.923) of the Langmuir model was higher than that of the Freundlich model, indicating that the adsorption of CTD on the multilayer β-CD/GO membrane could be monolayer adsorption and that the adsorption sites were homogeneous [54]. However, for SMZ and DCF, the higher correlation coefficients (R^2 = 0.984–0.988) obtained from the Freundlich model suggested that the adsorption for SMZ and DCF may be multilayered [55,56]. Moreover, the high R^2 value (R^2 > 0.97) of the Langmuir model indicated that the adsorption process of SMZ and DCF on the multilayer β-CD/GO membrane also involved monolayer adsorption [57]. The $1/n$ values were in the range of 0–1 (0.49–0.67), indicating that the adsorption of CTD, SMZ, and DCF on the multilayer β-CD/GO membrane was favorable [48]. According to the results of experimental data fitted with the Langmuir model, the maximum adsorption capacities of the multilayer β-CD/GO membrane for CTD, SMZ, and DCF were 35.56, 43.29, and 39.49 mg/g, respectively. It can be clearly seen from Table 3 that the adsorption capacity of the multilayer β-CD/GO membrane for PPCPs was higher than that of adsorbents reported in previous studies.

Table 2. Isothermal parameters of the multilayer β-CD/GO membrane for SMZ, CTD, and DCF adsorption.

Adsorption Kinetic Models	Parameters	PPCPs		
		CTD	SMZ	DCF
Langmuir	q_{max} (mg/g)	35.56	43.29	39.49
	K_L	0.388	0.081	0.042
	R^2	0.923	0.980	0.972
Freundlich	$1/n$	0.49	0.65	0.67
	K_F	9.404	4.170	2.368
	R^2	0.879	0.984	0.988

Table 3. Comparison of adsorption capacity of adsorbents reported in previous studies for PPCPs removal.

Adsorbents	q_{max} (mg/g)	Reference
Magnetic biochar	13.83	[34]
Magnetic biochar	9.42	[58]
Multiwalled carbon nanotubes	7.26	[59]
Pinewood biochar	0.53	[60]
Polydopamine–chitosan modified adsorbent	11.11	[61]

3.5. Adsorption Thermodynamics

The effect of temperature on the adsorption of CTD, SMZ, and DCF is shown in Figure 8. The maximum equilibrium adsorption capacities of CTD, SMZ, and DCF on the multilayer β-CD/GO membrane were measured at 298 K, with values of 29.00, 24.39,

and 18.78 mg/g, respectively. With the increase in temperature from 298 to 318 K, the adsorption capacities of CTD, SMZ, and DCF decreased to 21.85, 18.22, and 13.58 mg/g, corresponding to percentage reductions of 24.66%, 25.30%, and 27.69%, respectively.

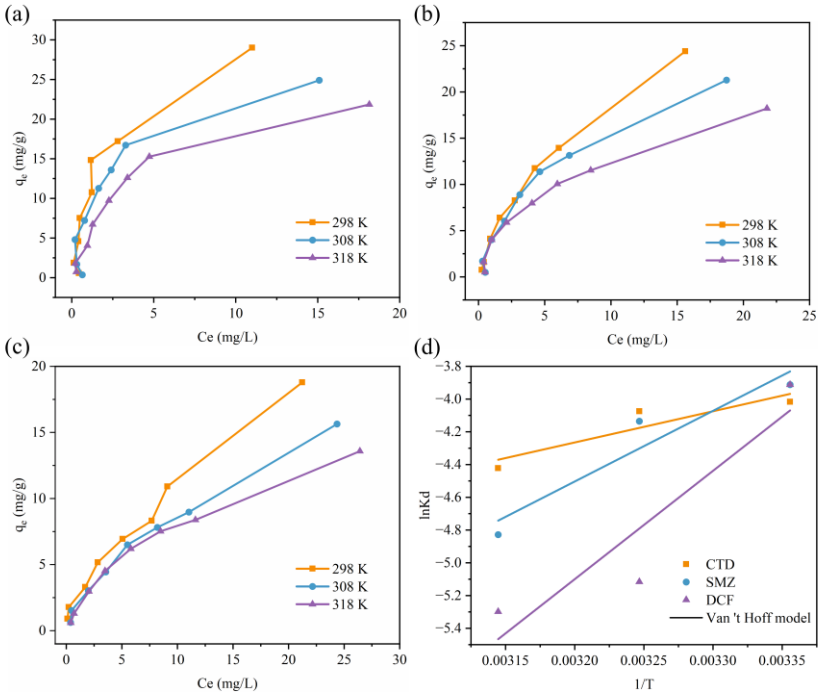

Figure 8. Effects of temperature on the adsorption of CTD (**a**), SMZ (**b**), and DCF (**c**) onto the multilayer β-CD/GO membrane. (**d**) Van 't Hoff plot for the adsorption of CTD, SMZ, and DCF onto the multilayer β-CD/GO membrane.

Thermodynamic studies can reveal the nature and spontaneity of the adsorption process of the multilayer β-CD/GO membrane for CTD, SMZ, and DCF. Thermodynamic parameters were calculated using Equations (6)–(8) [62].

$$lnK_d = -\frac{\Delta H^0}{RT} + \frac{\Delta S^0}{R}, \quad (6)$$

$$K_d = \frac{q_e}{C_e}, \quad (7)$$

$$\Delta G^0 = \Delta H^0 - T\Delta S^0, \quad (8)$$

where K_d is the thermodynamic equilibrium constant, R (8.314 J/mol·K) is the universal gas constant, T(K) is the absolute temperature, and ΔH^0 (kJ/mol), ΔS^0 (kJ/mol·K), and ΔG^0 (kJ/mol) represent the enthalpy, entropy, and Gibbs free energy, respectively.

The results of the thermodynamic parameters are listed in Table 4. The negative ΔH^0 values of −15.84 to −55.02 kJ/mol revealed that the adsorption was exothermic, indicating that lower temperatures favored the adsorption process [63]. The negative ΔS^0 values of −86.16 to −218.49 J/mol/K suggest that increasing temperature leads to a decrease in molecular randomness at the interface during the adsorption of PPCPs on the multilayer β-CD/GO membrane surface [64]. The positive ΔG^0 values for the adsorption of CTD, SMZ, and DCF were 9.84–11.56, 9.50–12.54, and 10.09–14.46 kJ/mol at 298–318 K, respectively, implying that the adsorption reaction was a non-spontaneous process [65]. In addition, the value of ΔG^0 increased with rising temperature, showing that the degree of non-spontaneity was positively correlated with temperature.

Table 4. Thermodynamic parameters of the multilayer β-CD/GO membrane for CTD, SMZ, and DCF adsorption at different temperatures.

PPCPs	Temperature (K)	ΔG^0 (kJ/mol)	ΔH^0 (kJ/mol)	ΔS^0 (J/mol/K)
CTD	298	9.84	−15.84	−86.16
	308	10.70		
	318	11.56		
SMZ	298	9.50	−35.88	−152.27
	308	11.02		
	318	12.54		
DCF	298	10.09	−55.02	−218.49
	308	12.27		
	318	14.46		

3.6. Effect of Coexisting Ions

The effects of coexisting ions on the adsorption performance of the multilayer β-CD/GO membrane for PPCPs are shown in Figure 9. The results indicate that the adsorption capacity of PPCPs was only slightly affected by the presence of coexisting ions. Compared to the concentration of 0 mol/L, the adsorption capacities of CTD, SMZ, and DCF slightly decreased to 7.42–9.29, 6.45–7.12, and 6.37–8.75 mg/g at 0.02 mol/L, respectively. With a further increase in concentration to 0.20 mol/L, the adsorption capacities of CTD, SMZ, and DCF marginally decreased to 4.88–6.45, 3.51–5.28, and 3.26–4.00 mg/g, respectively. This result may be due to the weakened electrostatic attraction between PPCPs and the multilayer β-CD/GO membrane, which was caused by the addition of coexisting ions [63]. In addition, the coexisting ions could occupy active adsorption sites on the multilayer β-CD/GO membrane through ion exchange with PPCPs, which hindered the complete adsorption of PPCPs [66]. At 0.02 mol/L, the adsorption of coexisting ions on the multilayer β-CD/GO membrane was saturated, and further increasing the ion concentration had no significant effect on the adsorption capacity of PPCPs. The negligible reduction in adsorption capacity was attributed to the increased viscosity and density of the aqueous solution at elevated ion concentrations, which hindered the mass transfer of PPCPs to the multilayer β-CD/GO membrane and thereby reduced the adsorption capacity [67].

For cations, Ca^{2+} inhibited the adsorption of PPCPs on the multilayer β-CD/GO membrane more strongly than Na^+. This finding was due to the fact that Na^+, as a monovalent cation, occupied only one vacancy on the β-CD/GO membrane, while Ca^{2+}, as a divalent cation, occupied two vacancies, thereby reducing the number of available adsorption sites for PPCPs [68–70]. In addition, Ca^{2+} reacted with -COOH in DCF via cation bridging to form complexes (Equation (9)), which weakened the electrostatic interactions and inhibited the formation of hydrogen bonds between DCF and the β-CD/GO membrane, causing a significant impediment to the adsorption of DCF [71,72]. In contrast, no clear trend was observed in the reduction in PPCP adsorption caused by the anions. The inhibitory effect of Cl^- on the adsorption of PPCPs could be attributed to the squeezing-out phenomenon [73]. Cl^- penetrated the multilayer structure of the β-CD/GO membrane, which made the membrane denser and thinner, possibly reducing its size. Meanwhile, the repulsive interactions between β-CD/GO membranes were weakened and even disappeared due to the presence of Cl^-, leading to the aggregation of the membrane, which is referred to as the squeezing-out phenomenon [69,73]. The high-density aggregated structure of the multilayer β-CD/GO membrane negatively affected the adsorption process of PPCPs. After CO_3^{2-} hydrolysis, the PPCP solution became alkaline [74]. The increasing solution pH values changed the ionization degree and existence state of PPCPs in solution. The adsorption capacity for PPCPs was reduced under alkaline conditions due to enhanced electrostatic repulsion, weakened hydrophobic and π-π EDA interactions, and inhibited hydrogen bond formation.

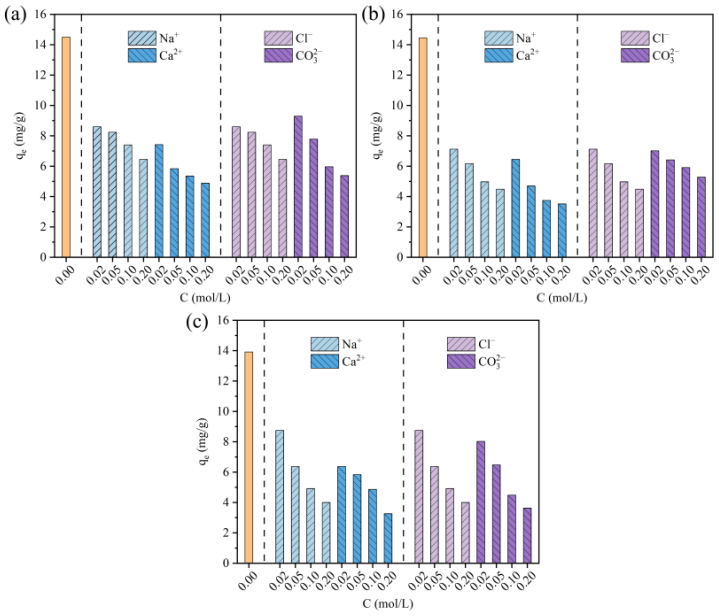

Figure 9. Effects of coexisting ions on the adsorption of CTD (**a**), SMZ (**b**), and DCF (**c**) onto the multilayer β-CD/GO membrane.

$$2R - COO^- + Ca^{2+} = Ca(RCOO)_2 \quad (9)$$

3.7. Regeneration of Multilayer β-CD/GO Membrane

The regeneration of the multilayer β-CD/GO membrane is an important factor in evaluating its practical applications. Five consecutive adsorption–desorption processes were performed for the multilayer β-CD/GO membrane under the same experimental conditions, and the results are shown in Figure 10. The adsorption capacities of CTD, SMZ, and DCF onto the multilayer β-CD/GO membrane during five consecutive cycles were 16.58–13.04, 11.59–8.05, and 13.32–9.78 mg/g, respectively. Compared to the first adsorption, the removal efficiencies of CTD, SMZ, and DCF declined by 21.83%, 24.52%, and 31.24%, respectively. The decrease in removal efficiency could be attributed to the reduction in available adsorption sites on the multilayer β-CD/GO membrane surface after each reuse. However, the removal efficiencies of the multilayer β-CD/GO membrane for CTD, SMZ, and DCF still remained at 58.45–71.73% after five cycles, which confirms the good regeneration ability of the multilayer β-CD/GO membrane.

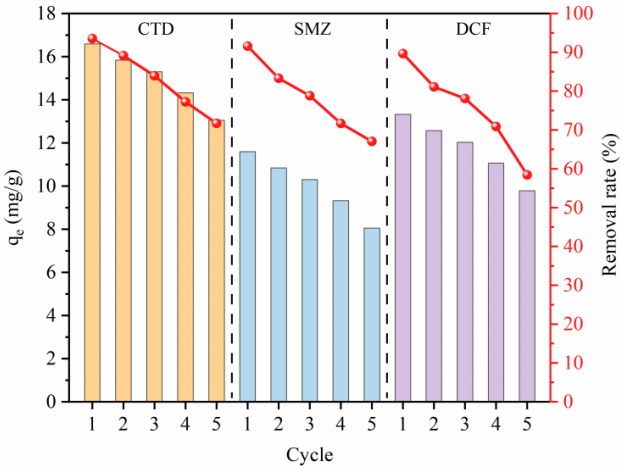

Figure 10. Effects of regeneration on the adsorption of CTD, SMZ, and DCF onto the multilayer β-CD/GO membrane.

4. Conclusions

In summary, a multilayer β-CD/GO membrane with a stable structure and target-selective adsorption of PPCPs was successfully prepared. The multilayer β-CD/GO membrane exhibited high adsorption performance for CTD, SMZ, and DCF with maximum capacities of 35.56, 43.29, and 39.49 mg/g, respectively, as determined by the Langmuir model. The optimal adsorption performance of the multilayer β-CD/GO membrane for PPCPs was observed at pH 4 and in the absence of coexisting ions. With increasing pH values in the range of 4–9, the adsorption capacities of CTD, SMZ, and DCF slightly decreased to 14.37, 13.69, and 13.01 mg/g, respectively, and the adsorption capacities decreased gradually to 4.88, 3.51, and 3.26 mg/g as the coexisting ion concentrations increased from 0 to 0.20 mol/L. The adsorption mechanisms involved electrostatic interactions, hydrogen bonding, hydrophobic interactions, and π-π EDA interactions. Combining kinetic and thermodynamic analyses, the adsorption of PPCPs onto a multilayer β-CD/GO membrane was a non-spontaneous process involving both physisorption and chemisorption. After five consecutive cycles, the adsorption of CTD, SMZ, and DCF by the multilayer β-CD/GO membrane remained at 13.04, 8.05, and 9.78 mg/g, respectively. Therefore, the multilayer β-CD/GO membrane can be used as an adsorbent for the effective removal of PPCPs from aqueous solutions due to its superior adsorption and regeneration performance.

Author Contributions: Conceptualization, Z.Z. and Y.Y.; methodology, Z.Z.; validation, Z.Z., Y.Y. and Z.T.; formal analysis, Z.T.; investigation, F.L.; resources, H.C.; data curation, F.L.; writing—original draft preparation, Y.Y.; writing—review and editing, Z.T.; visualization, H.C.; supervision, Y.Y.; funding acquisition, Z.Z. All authors have read and agreed to the published version of the manuscript.

Funding: This research was funded by the National Natural Science Foundation of China (No. 52370091). The authors are also grateful to the BUCEA Post Graduate Innovation Project and the Project of Construction and Support for High-Level Innovative Teams of Beijing Municipal Institutions (BPHR20220108).

Data Availability Statement: The data presented in this study are available on request from the corresponding author.

Conflicts of Interest: Author Fangyuan Liu was employed by Beijing SDL Technology Co., Ltd., and author Hongrui Chen was employed by CRRC Environmental Science & Technology Cooperation. The remaining authors declare that the research was conducted in the absence of any commercial or financial relationships that could be construed as a potential conflict of interest.

References

1. Gogoi, A.; Mazumder, P.; Tyagi, V.K.; Tushara Chaminda, G.G.; An, A.K.; Kumar, M. Occurrence and fate of emerging contaminants in water environment: A review. *Groundw. Sustain. Dev.* **2018**, *6*, 169–180. [CrossRef]
2. Subedi, B.; Balakrishna, K.; Joshua, D.I.; Kannan, K. Mass loading and removal of pharmaceuticals and personal care products including psychoactives, antihypertensives, and antibiotics in two sewage treatment plants in southern India. *Chemosphere* **2017**, *167*, 429–437. [CrossRef]
3. Ebele, A.J.; Abou-Elwafa Abdallah, M.; Harrad, S. Pharmaceuticals and personal care products (PPCPs) in the freshwater aquatic environment. *Emerg. Contam.* **2017**, *3*, 1–16. [CrossRef]
4. Kovalakova, P.; Cizmas, L.; McDonald, T.J.; Marsalek, B.; Feng, M.; Sharma, V.K. Occurrence and toxicity of antibiotics in the aquatic environment: A review. *Chemosphere* **2020**, *251*, 126351. [CrossRef]
5. Chen, W.; Xu, J.; Lu, S.; Jiao, W.; Wu, L.; Chang, A.C. Fates and transport of PPCPs in soil receiving reclaimed water irrigation. *Chemosphere* **2013**, *93*, 2621–2630. [CrossRef] [PubMed]
6. Xie, H.; Hao, H.; Xu, N.; Liang, X.; Gao, D.; Xu, Y.; Gao, Y.; Tao, H.; Wong, M. Pharmaceuticals and personal care products in water, sediments, aquatic organisms, and fish feeds in the Pearl River Delta: Occurrence, distribution, potential sources, and health risk assessment. *Sci. Total Environ.* **2019**, *659*, 230–239. [CrossRef] [PubMed]

7. Liu, N.; Jin, X.; Feng, C.; Wang, Z.; Wu, F.; Johnson, A.C.; Xiao, H.; Hollert, H.; Giesy, J.P. Ecological risk assessment of fifty pharmaceuticals and personal care products (PPCPs) in Chinese surface waters: A proposed multiple-level system. *Environ. Int.* **2020**, *136*, 105454. [CrossRef]
8. Tang, K.; Ooi, G.T.; Torresi, E.; Kaarsholm, K.M.; Hambly, A.; Sundmark, K.; Lindholst, S.; Sund, C.; Kragelund, C.; Christensson, M.; et al. Municipal wastewater treatment targeting pharmaceuticals by a pilot-scale hybrid attached biofilm and activated sludge system (Hybas™). *Chemosphere* **2020**, *259*, 127397. [CrossRef]
9. Adeoye, J.B.; Tan, Y.H.; Lau, S.Y.; Tan, Y.Y.; Chiong, T.; Mubarak, N.M.; Khalid, M. Advanced oxidation and biological integrated processes for pharmaceutical wastewater treatment: A review. *J. Environ. Manag.* **2024**, *353*, 120170. [CrossRef]
10. Xue, Y.; Sun, W.; Shao, P.; Yuan, Y.; Cui, F.; Shi, W. Degradation of contaminants of PPCPs by photocatalysis for water purification: Kinetics, mechanisms, and cytotoxicity analysis. *Chem. Eng. J.* **2023**, *454*, 140505. [CrossRef]
11. Tu, Y.; Han, L.; Ding, X.; Zhu, X.; Xu, G.; Xie, X.; Zhou, Q.; Shuang, C.; Li, A. Degradation of pharmaceuticals and personal care products (PPCPs) in municipal wastewater by white rot fungi: Neutral environment exploitation and degradation mechanisms. *Chem. Eng. J.* **2025**, *507*, 160794. [CrossRef]
12. Yin, Y.; Shi, M.; Ren, Y.; Wang, S.; Hua, M.; Lu, J.; Zhang, W.; Lv, L. Wrinkle structure on multifunctional MOFs to facilitate PPCPs adsorption in wastewater. *Chem. Eng. J.* **2020**, *387*, 124196. [CrossRef]
13. Fang, C.; Wang, S.; Xu, H.; Huang, Q. Degradation of tetracycline by atmospheric-pressure non-thermal plasma: Enhanced performance, degradation mechanism, and toxicity evaluation. *Sci. Total Environ.* **2022**, *812*, 152455. [CrossRef] [PubMed]
14. Dai, C.; Chen, D.; Wu, J.; Liu, J.; Shi, S.; Zhang, J.; Feng, Y. Construction of a novel integrated electrochemical oxidation-coagulation system for simultaneous removal of suspended solids and antibiotics. *Chem. Eng. J.* **2022**, *447*, 137505. [CrossRef]
15. Zhu, X.; He, M.; Sun, Y.; Xu, Z.; Wan, Z.; Hou, D.; Alessi, D.S.; Tsang, D.C. Insights into the adsorption of pharmaceuticals and personal care products (PPCPs) on biochar and activated carbon with the aid of machine learning. *J. Hazard. Mater.* **2022**, *423*, 127060. [CrossRef]
16. Zhang, H.; Huang, H.; Chen, W.; Zhang, Z.; Li, H.; Li, J. Mechanistic insight into efficient PPCPs removal on waste biological activated carbon for low-carbon emission reutilization. *Chem. Eng. J.* **2024**, *487*, 150759. [CrossRef]
17. Kumari, S.; Chowdhry, J.; Kumar, M.; Garg, M.C. Zeolites in wastewater treatment: A comprehensive review on scientometric analysis, adsorption mechanisms, and future prospects. *Environ. Res.* **2024**, *260*, 119782. [CrossRef]
18. Doan, T.H.Y.; Hoang, T.H.; Le, V.A.; Vu, D.N.; Vu, T.N.; Srivastav, A.L.; Pham, T.D. Adsorption and transformation of tetracyclines on alpha alumina particles with surface modification by anionic surfactant. *Environ. Res.* **2023**, *216*, 114618. [CrossRef]
19. Guo, L.; Xu, X.; Niu, C.; Wang, Q.; Park, J.; Zhou, L.; Lei, H.; Wang, X.; Yuan, X. Machine learning-based prediction and experimental validation of heavy metal adsorption capacity of bentonite. *Sci. Total Environ.* **2024**, *926*, 171986. [CrossRef]
20. Rahman, N.; Raheem, A. Adsorption of Cd(II) ions on magnetic graphene oxide/cellulose modified with β-cyclodextrin: Analytical interpretation via statistical physics modeling and fractal like kinetic approach. *Environ. Res.* **2024**, *243*, 117868. [CrossRef]
21. Jemli, S.; Pinto, D.; Kanhounnon, W.G.; Ben Amara, F.; Sellaoui, L.; Bonilla-Petriciolet, A.; Dhaouadi, F.; Ameri, R.; Silva, L.F.; Bejar, S.; et al. Green β-cyclodextrin nanosponges for the efficient adsorption of light rare earth elements: Cerium and lanthanum. *Chem. Eng. J.* **2023**, *466*, 143108. [CrossRef]
22. Mallard, I.; Städe, L.W.; Ruellan, S.; Jacobsen, P.A.L.; Larsen, K.L.; Fourmentin, S. Synthesis, characterization and sorption capacities toward organic pollutants of new β-cyclodextrin modified zeolite derivatives. *Colloids Surf. A Physicochem. Eng. Asp.* **2015**, *482*, 50–57. [CrossRef]
23. Huang, W.; Hu, Y.; Li, Y.; Zhou, Y.; Niu, D.; Lei, Z.; Zhang, Z. Citric acid-crosslinked β-cyclodextrin for simultaneous removal of bisphenol A, methylene blue and copper: The roles of cavity and surface functional groups. *J. Taiwan Inst. Chem. Eng.* **2018**, *82*, 189–197. [CrossRef]
24. Smith, A.T.; LaChance, A.M.; Zeng, S.; Liu, B.; Sun, L. Synthesis, properties, and applications of graphene oxide/reduced graphene oxide and their nanocomposites. *Nano Mater. Sci.* **2019**, *1*, 31–47. [CrossRef]
25. Sun, M.; Li, J. Graphene oxide membranes: Functional structures, preparation and environmental applications. *Nano Today* **2018**, *20*, 121–137. [CrossRef]
26. Peng, G.; Zhang, M.; Deng, S.; Shan, D.; He, Q.; Yu, G. Adsorption and catalytic oxidation of pharmaceuticals by nitrogen-doped reduced graphene oxide/Fe3O4 nanocomposite. *Chem. Eng. J.* **2018**, *341*, 361–370. [CrossRef]
27. Ersan, G.; Apul, O.G.; Perreault, F.; Karanfil, T. Adsorption of organic contaminants by graphene nanosheets: A review. *Water Res.* **2017**, *126*, 385–398. [CrossRef]
28. Chen, J.; Yao, B.; Li, C.; Shi, G. An improved Hummers method for eco-friendly synthesis of graphene oxide. *Carbon* **2013**, *64*, 225–229. [CrossRef]

29. Jiang, S.; Wang, Q.; Wang, Z.; Borjigin, G.; Sun, J.; Zhao, Y.; Li, Q.; Shi, X.; Shah, S.F.A.; Wang, X.; et al. Ultrasound-assisted polysaccharide extraction from Fritillaria ussuriensis Maxim. and its structural characterization, antioxidant and immunological activity. *Ultrason. Sonochem.* **2024**, *103*, 106800. [CrossRef]
30. Zhou, W.; Zhang, W.; Cai, Y. Enzyme-enhanced adsorption of laccase immobilized graphene oxide for micro-pollutant removal. *Sep. Purif. Technol.* **2022**, *294*, 121178. [CrossRef]
31. Zhang, Z.; Wang, W.; Liu, F.; Chen, H.; Zhang, X.; Tan, C.; Gong, Y. Removal Efficiency and Mechanism of Typical PPCPs onto Novel Cyclodextrin–Graphene Oxide Composite Adsorbent in Aqueous Solutions. *Water* **2025**, *17*, 590. [CrossRef]
32. Maeng, S.K.; Cho, K.; Jeong, B.; Lee, J.; Lee, Y.; Lee, C.; Choi, K.J.; Hong, S.W. Substrate-immobilized electrospun TiO2 nanofibers for photocatalytic degradation of pharmaceuticals: The effects of pH and dissolved organic matter characteristics. *Water Res.* **2015**, *86*, 25–34. [CrossRef] [PubMed]
33. Ahmed, M.B.; Zhou, J.L.; Ngo, H.H.; Guo, W.; Johir, M.A.H.; Belhaj, D. Competitive sorption affinity of sulfonamides and chloramphenicol antibiotics toward functionalized biochar for water and wastewater treatment. *Bioresour. Technol.* **2017**, *238*, 306–312. [CrossRef]
34. Reguyal, F.; Sarmah, A.K.; Gao, W. Synthesis of magnetic biochar from pine sawdust via oxidative hydrolysis of FeCl2 for the removal sulfamethoxazole from aqueous solution. *J. Hazard. Mater.* **2017**, *321*, 868–878. [CrossRef]
35. Zeng, S.; Choi, Y.-K.; Kan, E. Iron-activated bermudagrass-derived biochar for adsorption of aqueous sulfamethoxazole: Effects of iron impregnation ratio on biochar properties, adsorption, and regeneration. *Sci. Total Environ.* **2021**, *750*, 141691. [CrossRef] [PubMed]
36. Choi, Y.-K.; Kan, E. Effects of pyrolysis temperature on the physicochemical properties of alfalfa-derived biochar for the adsorption of bisphenol A and sulfamethoxazole in water. *Chemosphere* **2019**, *218*, 741–748. [CrossRef] [PubMed]
37. Keiluweit, M.; Kleber, M. Molecular-Level Interactions in Soils and Sediments: The Role of Aromatic π-Systems. *Environ. Sci. Technol.* **2009**, *43*, 3421–3429. [CrossRef]
38. Pan, B.; Xing, B. Adsorption Mechanisms of Organic Chemicals on Carbon Nanotubes. *Environ. Sci. Technol.* **2008**, *42*, 9005–9013. [CrossRef]
39. Peiris, C.; Gunatilake, S.R.; Mlsna, T.E.; Mohan, D.; Vithanage, M. Biochar based removal of antibiotic sulfonamides and tetracyclines in aquatic environments: A critical review. *Bioresour. Technol.* **2017**, *246*, 150–159. [CrossRef]
40. Wang, Y.; Jiao, W.-B.; Wang, J.-T.; Liu, G.-F.; Cao, H.-L.; Lü, J. Amino-functionalized biomass-derived porous carbons with enhanced aqueous adsorption affinity and sensitivity of sulfonamide antibiotics. *Bioresour. Technol.* **2019**, *277*, 128–135. [CrossRef]
41. Lv, M.; Li, D.; Zhang, Z.; Logan, B.E.; Liu, G.; Sun, M.; Dai, C.; Feng, Y. Unveiling the correlation of Fe3O4 fractions upon the adsorption behavior of sulfamethoxazole on magnetic activated carbon. *Sci. Total Environ.* **2021**, *757*, 143717. [CrossRef] [PubMed]
42. Yao, Y.; Zhang, Y.; Gao, B.; Chen, R.; Wu, F. Removal of sulfamethoxazole (SMX) and sulfapyridine (SPY) from aqueous solutions by biochars derived from anaerobically digested bagasse. *Environ. Sci. Pollut. Res.* **2018**, *25*, 25659–25667. [CrossRef]
43. Xie, M.; Chen, W.; Xu, Z.; Zheng, S.; Zhu, D. Adsorption of sulfonamides to demineralized pine wood biochars prepared under different thermochemical conditions. *Environ. Pollut.* **2014**, *186*, 187–194. [CrossRef]
44. Ahmed, M.B.; Zhou, J.L.; Ngo, H.H.; Guo, W.; Johir, M.A.H.; Sornalingam, K. Single and competitive sorption properties and mechanism of functionalized biochar for removing sulfonamide antibiotics from water. *Chem. Eng. J.* **2017**, *311*, 348–358. [CrossRef]
45. Zheng, H.; Wang, Z.; Zhao, J.; Herbert, S.; Xing, B. Sorption of antibiotic sulfamethoxazole varies with biochars produced at different temperatures. *Environ. Pollut.* **2013**, *181*, 60–67. [CrossRef]
46. Rahman, N.; Raheem, A.; Nasir, M.; Franco, D.S. Fractal-like kinetic modelling for sorption of diclofenac onto graphene oxide/polypyrrole composite: Mechanism analysis and response surface methodology for optimization. *Diam. Relat. Mater.* **2023**, *139*, 110328. [CrossRef]
47. Hu, C.; Jiang, J.; An, Y.; Jiang, X.; Sun, Q.; Zheng, H.; Li, H. A novel self-floating silica adsorbent for antibiotic ciprofloxacin and nickel (II) ion. *Chem. Eng. J.* **2022**, *429*, 132227. [CrossRef]
48. Wang, R.; Yao, C.; Peng, C.; Qiu, J.; Wang, Q.; Liu, X.; Meng, J.; Wang, W. Ultra-strong adsorption of organic dyes and antibiotic onto the alk-MXene/ZIF adsorbents with a specific intercalation structure. *Chem. Eng. J.* **2024**, *485*, 149916. [CrossRef]
49. Yadav, S.; Asthana, A.; Singh, A.K.; Chakraborty, R.; Vidya, S.S.; Susan, A.B.H.; Carabineiro, S.A. Adsorption of cationic dyes, drugs and metal from aqueous solutions using a polymer composite of magnetic/β-cyclodextrin/activated charcoal/Na alginate: Isotherm, kinetics and regeneration studies. *J. Hazard. Mater.* **2021**, *409*, 124840. [CrossRef]
50. Liu, B.; Chen, T.; Wang, B.; Zhou, S.; Zhang, Z.; Li, Y.; Pan, X.; Wang, N. Enhanced removal of Cd2+ from water by AHP-pretreated biochar: Adsorption performance and mechanism. *J. Hazard. Mater.* **2022**, *438*, 129467. [CrossRef]

51. Huang, Y.; Zheng, H.; Li, H.; Zhang, Z.; Zhao, C.; Gou, Q.; Liu, Y. Highly effective and selective adsorption of thorium(IV) from aqueous solution using mesoporous graphite carbon nitride prepared by sol–gel template method. *Chem. Eng. J.* **2021**, *410*, 128321. [CrossRef]
52. Yao, N.; Li, C.; Yu, J.; Xu, Q.; Wei, S.; Tian, Z.; Yang, Z.; Yang, W.; Shen, J. Insight into adsorption of combined antibiotic-heavy metal contaminants on graphene oxide in water. *Sep. Purif. Technol.* **2020**, *236*, 116278. [CrossRef]
53. Hamza, M.F.; Hamad, D.M.; Hamad, N.A.; Abdel-Rahman, A.A.-H.; Fouda, A.; Wei, Y.; Guibal, E.; El-Etrawy, A.-A.S. Functionalization of magnetic chitosan microparticles for high-performance removal of chromate from aqueous solutions and tannery effluent. *Chem. Eng. J.* **2022**, *428*, 131775. [CrossRef]
54. Jiao, C.; Wang, Y.; Li, M.; Wu, Q.; Wang, C.; Wang, Z. Synthesis of magnetic nanoporous carbon from metal-organic framework for the fast removal of organic dye from aqueous solution. *J. Magn. Magn. Mater.* **2016**, *407*, 24–30. [CrossRef]
55. Yao, M.; Zhang, G.; Shao, D.; Ding, S.; Li, L.; Li, H.; Zhou, C.; Luo, B.; Lu, L. Preparation of chitin/MXene/poly(L-arginine) composite aerogel spheres for specific adsorption of bilirubin. *Int. J. Biol. Macromol.* **2023**, *243*, 125140. [CrossRef]
56. Fan, W.; Xin, Q.; Dai, Y.; Chen, Y.; Liu, S.; Zhang, X.; Yang, Y.; Gao, X. Competitive transport and adsorption of CO2/H2O in the graphene nano-slit pore: A molecular dynamics simulation study. *Sep. Purif. Technol.* **2025**, *353*, 128394. [CrossRef]
57. Park, S.; Kim, S.; Yea, Y.; Saravanakumar, K.; Lee, E.; Yoon, Y.; Park, C.M. Adsorptive and photocatalytic performance of cobalt-doped ZnTiO3/Ti3C2Tx MXene nanohybrids towards tetracycline: Kinetics and mechanistic insight. *J. Hazard. Mater.* **2023**, *443*, 130165. [CrossRef]
58. Reguyal, F.; Sarmah, A.K. Adsorption of sulfamethoxazole by magnetic biochar: Effects of pH, ionic strength, natural organic matter and 17α-ethinylestradiol. *Sci. Total Environ.* **2018**, *628–629*, 722–730. [CrossRef]
59. Gil, A.; Santamaría, L.; Korili, S. Removal of Caffeine and Diclofenac from Aqueous Solution by Adsorption on Multiwalled Carbon Nanotubes. *Colloid Interface Sci. Commun.* **2018**, *22*, 25–28. [CrossRef]
60. Lonappan, L.; Rouissi, T.; Brar, S.K.; Verma, M.; Surampalli, R.Y. An insight into the adsorption of diclofenac on different biochars: Mechanisms, surface chemistry, and thermodynamics. *Bioresour. Technol.* **2018**, *249*, 386–394. [CrossRef]
61. Sun, M.; Sun, Q.; Zhao, C.; Huang, Y.; Jiang, J.; Ding, W.; Zheng, H. Degradation of diclofenac sodium with low concentration from aqueous milieu through polydopamine-chitosan modified magnetic adsorbent-assisted photo-Fenton process. *Sep. Purif. Technol.* **2022**, *289*, 120771. [CrossRef]
62. Azqandi, M.; Ramavandi, B.; Nasseh, N.; Zaarei, D.; Fanaei, F. Green synthesis of manganese ferrite magnetic nanoparticle and its modification with metallic-organic frameworks for the tetracycline adsorption from aqueous solutions: A mathematical study of kinetics, isotherms, and thermodynamics. *Environ. Res.* **2024**, *256*, 118957. [CrossRef]
63. Li, C.; Wang, F.; Xu, X.; Shi, Y.; Liang, J.; Yang, R.; Liu, J.; Zhao, Z. A high-capacity malleable cellulose aerogel with layered double hydroxide decorating ZIF-8 for efficient adsorption of ciprofloxacin. *Chem. Eng. J.* **2023**, *455*, 140841. [CrossRef]
64. Tang, M.; Jia, R.; Kan, H.; Liu, Z.; Yang, S.; Sun, L.; Yang, Y. Kinetic, isotherm, and thermodynamic studies of the adsorption of dye from aqueous solution by propylene glycol adipate-modified cellulose aerogel. *Colloids Surf. A Physicochem. Eng. Asp.* **2020**, *602*, 125009. [CrossRef]
65. Du, R.; Cao, H.; Wang, G.; Dou, K.; Tsidaeva, N.; Wang, W. PVP modified rGO/CoFe2O4 magnetic adsorbents with a unique sandwich structure and superior adsorption performance for anionic and cationic dyes. *Sep. Purif. Technol.* **2022**, *286*, 120484. [CrossRef]
66. Kong, X.; Feng, S.; Zhang, X.; Li, Y. Effects of bile salts and divalent cations on the adsorption of norfloxacin by agricultural soils. *J. Environ. Sci.* **2014**, *26*, 846–854. [CrossRef]
67. Wu, G.; Ma, J.; Li, S.; Guan, J.; Jiang, B.; Wang, L.; Li, J.; Wang, X.; Chen, L. Magnetic copper-based metal organic framework as an effective and recyclable adsorbent for removal of two fluoroquinolone antibiotics from aqueous solutions. *J. Colloid Interface Sci.* **2018**, *528*, 360–371. [CrossRef]
68. Zhao, Y.; Geng, J.; Wang, X.; Gu, X.; Gao, S. Adsorption of tetracycline onto goethite in the presence of metal cations and humic substances. *J. Colloid Interface Sci.* **2011**, *361*, 247–251. [CrossRef]
69. Xie, J.; Liu, M.; He, M.; Liu, Y.; Li, J.; Yu, F.; Lv, Y.; Lin, C.; Ye, X. Ultra-efficient adsorption of diclofenac sodium on fish-scale biochar functionalized with H3PO4 via synergistic mechanisms. *Environ. Pollut.* **2023**, *322*, 121226. [CrossRef]
70. Dou, S.; Ke, X.-X.; Shao, Z.-D.; Zhong, L.-B.; Zhao, Q.-B.; Zheng, Y.-M. Fish scale-based biochar with defined pore size and ultrahigh specific surface area for highly efficient adsorption of ciprofloxacin. *Chemosphere* **2022**, *287*, 131962. [CrossRef]
71. Zhang, Y.; Zhu, C.; Liu, F.; Yuan, Y.; Wu, H.; Li, A. Effects of ionic strength on removal of toxic pollutants from aqueous media with multifarious adsorbents: A review. *Sci. Total Environ.* **2019**, *646*, 265–279. [CrossRef] [PubMed]
72. Yang, W.; Lu, Y.; Zheng, F.; Xue, X.; Li, N.; Liu, D. Adsorption behavior and mechanisms of norfloxacin onto porous resins and carbon nanotube. *Chem. Eng. J.* **2012**, *179*, 112–118. [CrossRef]

73. Jiang, L.; Liu, Y.; Liu, S.; Hu, X.; Zeng, G.; Hu, X.; Liu, S.; Liu, S.; Huang, B.; Li, M. Fabrication of β-cyclodextrin/poly (l-glutamic acid) supported magnetic graphene oxide and its adsorption behavior for 17β-estradiol. *Chem. Eng. J.* **2017**, *308*, 597–605. [CrossRef]
74. Roy, N.; Kannabiran, K.; Mukherjee, A. Integrated adsorption and photocatalytic degradation based removal of ciprofloxacin and sulfamethoxazole antibiotics using Fc@rGO-ZnO nanocomposite in aqueous systems. *Chemosphere* **2023**, *333*, 138912. [CrossRef] [PubMed]

Disclaimer/Publisher's Note: The statements, opinions and data contained in all publications are solely those of the individual author(s) and contributor(s) and not of MDPI and/or the editor(s). MDPI and/or the editor(s) disclaim responsibility for any injury to people or property resulting from any ideas, methods, instructions or products referred to in the content.